3D MOTION IN MAGNETIC ACTUATOR MODELLING

Philippe Wendling
Magsoft Corporation
Troy, NY USA

Patrick Lombard, Richard Ruiz, Christophe Guerin
Cedrat
Meylan, France

Vincent Leconte
Corporate Research and Development
Schneider Electric
Grenoble, France

Christian Bataille
Schneider Electric
Nanterre, France

Abstract - *This paper presents new 3D modelling schemes for the analysis of magnetic actuators. The modelling takes into account the interactions between the motion of the rigid body, the external circuit coupling and the finite element EM computation. A new technique has been developed to handle both translating and pivoting motion. These new schemes have been validated on an E-shaped magnetic actuator provided by Schneider Electric*

I. INTRODUCTION

Until recently, the computation of devices with motion through 3D electromagnetic modelling programs was limited to the computation of rotating machines [1] [2] [3]. The modelling of the rotating motion of rigid bodies is commonly performed with one of two methods. The first method is based on the use of a sliding cylindrical surface, where the nodes along the surface are duplicated on both sides of the surface, one set of nodes associated with the stator and not moving, the other associated with the rotor and moving. The second method calls for the coupling between the finite element method (FEM) and the boundary element method (BEM), so that the entire domain, except for the airgap associated with the motion, is modelled using finite elements, while the airgap associated with the motion is modelled using boundary elements [4]. In both these methods, the motion is well understood because it can occur only about a centre axis of rotating motion, usually the centre of the rotor. The part of the domain affected by the motion, usually the airgap of the rotating machine, has a set and invariant shape.

For other types of motion, such as translating or pivoting motion, the challenge of defining the problem is greater because the part affected by the motion changes in shape. For translating motion, the shape is extended on one side of the moving object while being compressed on the other side. For pivoting motion, the modifications carried out on the shape are even more complex.

Today, most of the computations are performed as multi-static samples. In this case, the problem is computed for independent relative positions of the moving part versus the rest of the domain. For each position, the geometry is modified and meshed and the problem is solved. An equivalent lumped

parameter model is derived from this multi-position treatment and processed in a system simulation tool for the dynamic study of the device. With such a simulation, it is rather difficult to precisely take into account the dynamic effects of the motion on the EM part of the problem, i.e., the development of eddy currents in the conducting part due to the motion of the piece through a magnetic field. These dynamic effects are key elements in the operation of safety equipment because they may delay the opening of switches and lead to complex failures of systems. It is also necessary to take into account these dynamic effects when modelling linear machines and similar types of devices such as magnetic launchers [5] [6] [7].

In the new modelling schemes presented in this paper, we propose to include the translating or pivoting motion within the magnetic finite element analysis, and to connect this finite element problem with external circuits. These new modelling techniques will take into account all of the dynamic effects of the motion, including the eddy currents generated by the motion.

II. DEFINING THE MOTION IN THE 3D PROBLEM

To define the motion in this new modelling technique, most of the volume regions of the domain are identified either as part of the nonmoving mechanical set, or as part of the moving mechanical set. To model the remaining region surrounding the moving mechanical set, the airgap (which is in fact the region being affected by the motion), we tested a boundary BEM formulation. We found that the CPU time needed by commonly used computers (1 GHz processor speed, up to 2GB of RAM) for the computation of the FEM/BEM problem was not acceptable. Furthermore, accuracy problems developed for very small sizes of the airgap. In view of these impediments, a re-meshing scheme [8] was chosen for the airgap region. Later in this paper, we refer to this airgap as the “compressible” region.

In our new modelling scheme, the moving mechanical set has either a translating or a pivoting motion. The mesh in the nonmoving set and in the moving set is kept intact through the motion. No re-meshing is performed in these parts of the domain. The meshing of the compressible region is redone at each new position, adapting to the new shape of the compressible set. At each new position, the following steps are completed:

- Delete the compressible mesh
- Move the moving part according to the mechanical equation (keeping geometry and mesh intact)
- Re-mesh the compressible region, and only that region, and store this new mesh information
- Connect this mesh to the stored mesh of the moving and nonmoving sets.

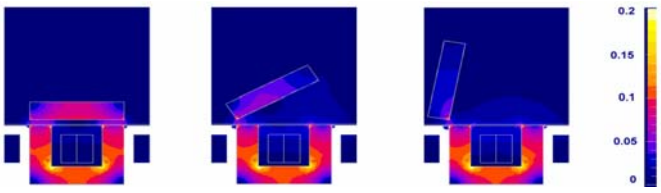

Figure #1. Pivoting motion – Flux density distribution for 3 positions of the pivoting object.

By proceeding in this manner, it is very easy to handle both translating and pivoting motion. Figure #1 shows three positions of the moving part in the dynamic study of an actuator with a pivoting blade.

Figure #2 shows the 3D geometry and the mesh, for two positions of the moving part. The compressible region is displayed in yellow. Only the mesh in the compressible region is changed from one figure to the next.

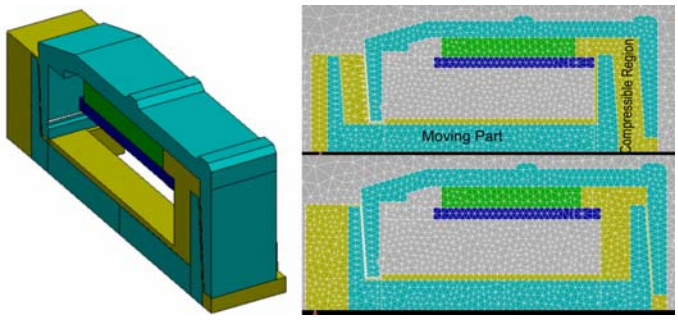

Figure #2. Translating motion – Geometry and mesh for two positions of the moving part..

In the specific case of translating motion without the need for a compressible region, another method is applied, more similar to one of the methods used to model rotating motion. This method applies to linear motors and similar devices. A planar sliding surface is created between the moving and the nonmoving parts of the domain. The nodes along the surface are duplicated on both sides of the surface, one set of nodes associated with the nonmoving part, the other associated with the moving part. The mesh stays the same throughout the whole computation. A specific interface boundary condition is used along the sliding surface. Periodic boundary conditions can also be applied along the same surface. Using this method, if the geometry and the physics of the problem permit it, it is possible to model only one pole, as would be done for a rotating machine problem. An example of this type of modelling is shown in Figure #3.

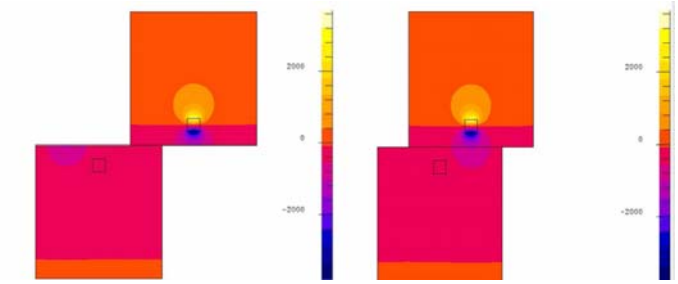

Figure #3. Translating motion, sliding surface – Flux density distribution in Tesla for 2 positions of the moving object

III. 3D MOTION: MECHANICAL EQUATION

The different types of motion described in the previous section and their associate methods are available to compute multi-static samples, constant speed problems and mechanical coupling. For multi-static sample computation, it is very easy to create a position sampling and let the program deal with all the aspects of the motion. In this case of course, the computation yields only disconnected static samples of the problem.

For the constant speed computation, the speed is defined by the user. The program computes the time transient solution including the effect of the motion on the EM part of the problem. The position of the moving part is, however, determined solely by the speed and the time sample.

For the mechanical coupling, one more equation is needed to compute the acceleration, the speed and the position of the moving part. The time transient problem is solved, including the effect of the motion. At each time sample, the magnetic force is computed and applied to the mechanical equation to calculate the speed and the position for the next time step. The mechanical equations, depending on the type of motion, are:

$$m.(d2x/dt2) = \tilde{\Gamma_e} - \Gamma_{f\_ext} \quad (1)$$

$$J.(d^2\theta/dt^2) = \tilde{\Gamma_e} - \Gamma_{f\_ext} \quad (2)$$

In translating motion (1), m is the mass of the moving part, x the motion, Γ_e the electromagnetic force computed from the FEM analysis, Γ_{f_ext} the sum of the external loads:

$$\Gamma_{f\_ext} = f_0.sign(dx/d\tilde{t}) - f_1.(dx/d\tilde{t}) - f_2.(dx/dt)^2.sign(dx/dt) \quad (3)$$

In pivoting motion (2), J is the moment of inertia of the moving part versus its pivot axis, θ the angular motion, Γ_e the electromagnetic torque versus the pivot point, computed from the FEM analysis, and Γ_{f_ext} the sum of the external loads:

$$\Gamma_{f\_ext} = f_0.sign(d\theta/d\tilde{t}) - f_1.(d\theta/d\tilde{t}) - f_2.(d\theta/dt)^2.sign(d\theta/dt) \quad (4)$$

In both cases (3) and (4), the external loads are the summations of the load force or torque f_0, the viscous friction f_1 and the friction associated with the speed squared f_2. The function sign takes the sign of the speed in this case.

To solve the mechanical equation, an initial solving is performed to compute the forces or torques developed in the electromagnetic domain. Once these quantities are known, the program solves the mechanical equations. These algorithms are well known and commonly used by tools solving the coupled electromagnetic mechanical problem for rotating motion. Here they are applied to translating and pivoting motion.

Because the translating or pivoting motions have no end in range, contrary to the rotating motion, a mechanical stop function has been added to this new modelling scheme. This mechanical stop sets limits to the range of motion for the moving part. In fact, these limits are necessary to take into account any part of the device that has no magnetic influence and would be modelled as vacuum or not represented in the magnetic analysis.

We will now concentrate exclusively on the 3D translating motion associated with the compressible part. The validation of the pivoting motion is shown in another presentation. To validate the 3D translating motion, this new modelling technique, implemented in FLUX, has been applied first to examples having an analytical solution, then to examples solved with the already existing and validated 2D translating capabilities of FLUX. Finally, a "real world" validation was conducted on an existing device for which results were compared to measurements. The interest of the first part of the validation does not warrant presentation in this paper. We will present the validation with 2D solutions and, of course, the real-world validation.

IV. VALIDATION BY COMPARISON OF 2D AND 3D SOLUTIONS

To validate the 3D implementation of these new modelling techniques, we performed the 2D analysis of an actuator both in the 2D and the 3D environments. The 2D translating capabilities have already been validated for several years and are commonly used today [9]. The results obtained in the 3D environment were compared to the results obtained in the 2D environment. The device chosen for this validation is a standard actuator. A full computation with mechanical coupling and external circuit connections is used for the validation.

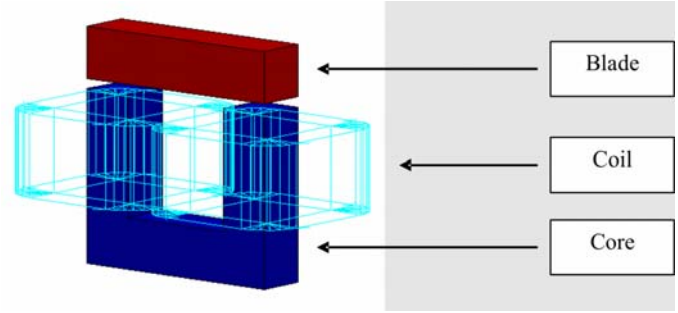

Figure #4. Geometry of the Actuator

The geometry, shown in Figure #4, includes a U-shaped magnetic core and one coil associated with the nonmoving part of the domain, a movable blade associated with the moving part of the domain, and the airgap associated with the compressible part of the domain. The rest of the domain is air, associated with the nonmoving part of the domain. The Geometric Domain defined to perform the modelling in both the 2D and 3D environments is shown in Figure #5.

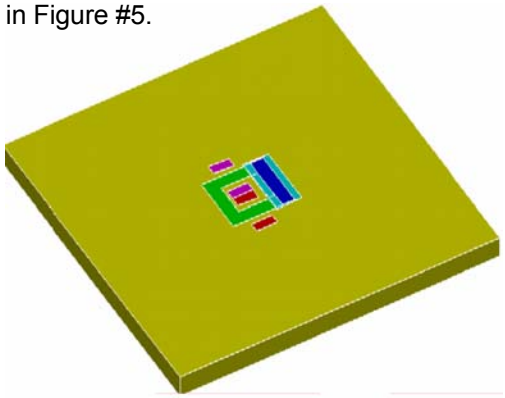

Figure #5. Geometric Domain of the 2D–3D Test Case

The coils of the actuator are connected to an external circuit. The circuit includes a DC voltage source, a stranded coil element and a lumped resistor holding the resistance of the coil. This circuit is shown in Figure #6.

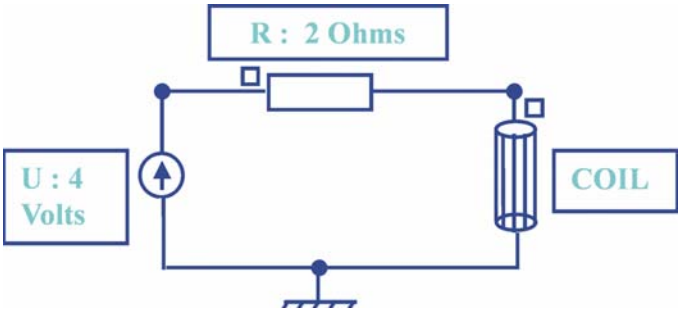

Figure #6. External Circuit Associated to the Actuator

At the start of the computation, the quantities are all initialized to zero and no current is flowing in the circuit. As the current establishes itself in the circuit and increases, the moving part begins to move, to close the airgap. We compare the results obtained in the 2D environment to the results obtained in the 3D environment. The values of the current in the circuit and the position of the moving part versus time are the items of interest.

The curve of the position of the moving part versus time is shown in Figure #7. As expected, the results obtained in the 3D environment are identical to the results obtained in the 2D environment.

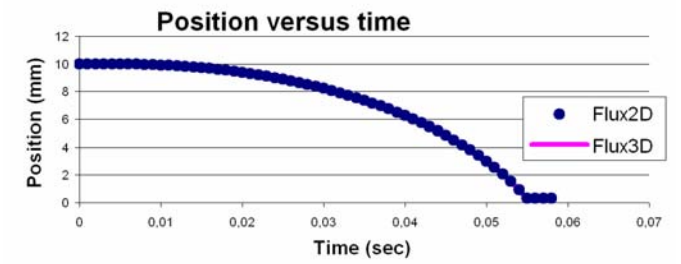

Figure #7. 2D – 3D Computed Position of Moving Part vs. Time

From the shape of the current in the circuit (or the domain), it is easy to identify when the moving part stops moving. When the motion is completed, the shape of the current becomes the one expected in a common R-L circuit. Again, the values for the currents computed in the 3D environment are very close to the values of the current computed in the 2D environment.

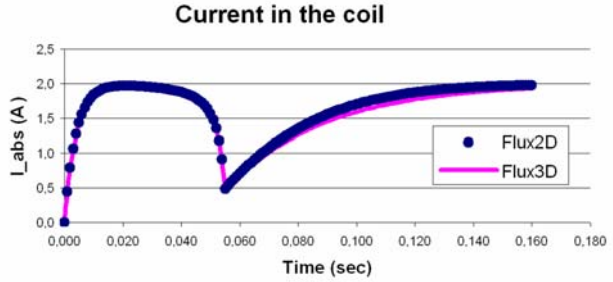

Figure #8. 2D – 3D Computed Current in the Circuit vs. Time

This validates the 3D implementation of the translating airgap. For further validation, this new technique is applied to a real device.

V. APPLICATION TO A REAL ACTUATOR: COMPUTATION AND MEASUREMENT

The device chosen for this validation is a commonly used actuator for opening or closing a power switch. It is a well-known device. The geometry of the device is shown in Figure #9. This device operates in a way similar to the one shown in the previous section.

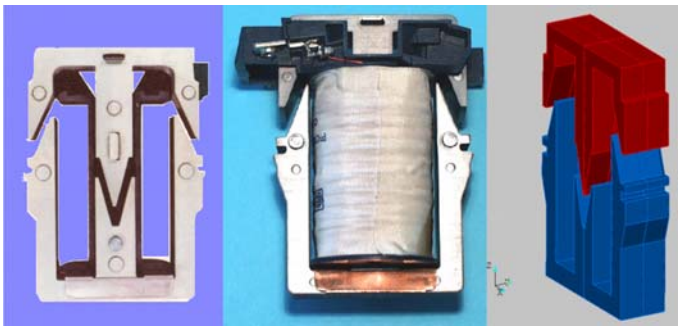

Figure #9. Actuator and Associated Geometry

A constant DC Voltage is applied to the terminals of the coil to close the device. When no voltage is applied, a spring brings the moving part back to its original open position. An external circuit connection is used to define the electrical components associated with the device. The circuit consists of a DC voltage, a coil and a lumped resistor holding the resistance of the winding. The circuit and its characteristics are shown in Figure #10. When the computation starts, the current rises, and the blade moves to close the air gap.

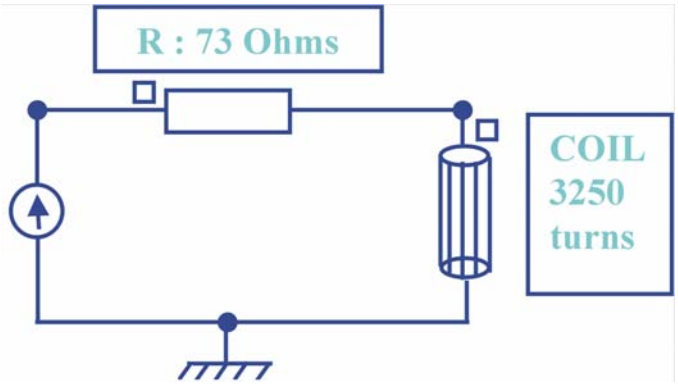

Figure #10. External Circuit Associated with the Actuator

The spring attached to the moving blade does not have a constant stiffness. From a set of static measurements performed on the device, we obtain the variation of the force exerted by the spring versus the position of the blade. This variation is shown in Figure #11.

The model of the force versus position is limited to a motion of the blade of 6 mm. This is the range of motion shown by the device. The spring exerts the highest forces at the closing of the airgap. These forces are difficult to measure accurately.

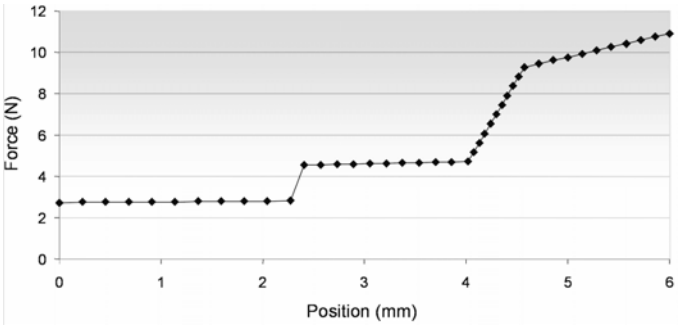

Figure #11. Variation of the Force in N versus Position of the Blade

During the solving, the force on the blade is read from a table and included in the mechanical equation as a load force on the moving part. It is read for each position of the blade.

The other measured data, available from the experiments on the device, are the current and the position, measured for static positions and for dynamic motion, and the force measured for dynamic motion.

Because of the symmetries in the geometry and in the physics of the device, the domain is reduced to only one quarter of the geometry. Figure #12 shows the magnetic components of the device as meshed regions and the associated coil. The part shown at the top of the figure is the moving part. The compressible region is located within the two parts of the airgap between the two magnetic regions. The air region is not shown in this figure. The magnetic regions are made of laminated steel. A nonlinear B(H) curve characterizes the material and is included in the model. Because the regions are laminated, no eddy currents are included in this study.

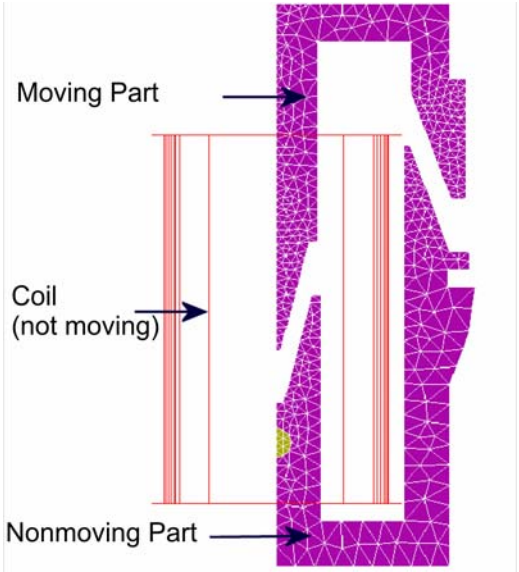

Figure #12. Geometry and Mesh of the Actuator

The 3D time transient simulation, with mechanical and external circuit couplings, was conducted for different values of the voltage applied to the coil. The curve of position of the blade versus time had a similar shape in all of these simulations. Of course, for a higher voltage, a faster motion was computed. Figure #13 shows the curve of position of the blade versus time for a voltage of 24 V along with the related measurements. There is very good agreement between the measurements and the results of the computation. We offer two comments on these results:

- the recoil of the moving part at the closing of the actuator is missed by the computation. One possible explanation is the lack of accurate measured data on the force exerted by the spring at closing.
- the speed computed is slightly higher than the speed observed during the measurement. The modelling of the load forces, including dissipative friction, can certainly be improved.

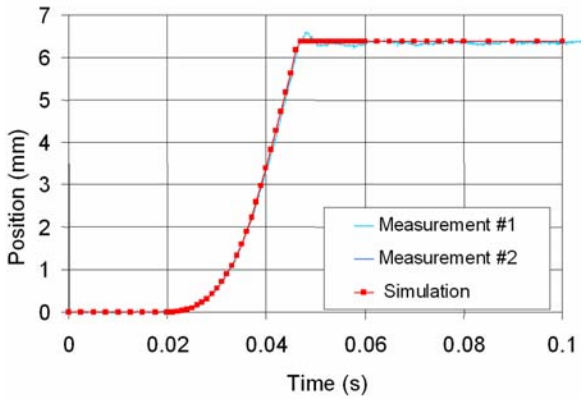

Figure #13. Position of the Moving Part vs. Time – V = 24VDC

The kinetic energy calculated from the measured speed and the speed obtained from the modelling show good agreement. However, the measurements of the speed on the device are too imprecise at this point to merit any interest in this result.

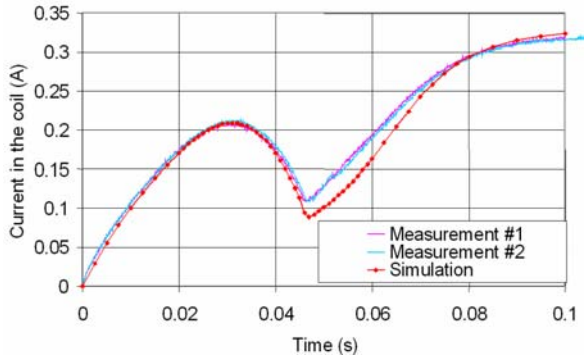

Figure #14. Curve of Current vs. Time – V = 24 VDC

The comparison between the measured and computed currents in the circuit is shown in Figure #14. The shapes of the curves show good agreement between the measurement and the computation. The

difference in the current is shown at impact. This confirms the information seen on the curve of position versus time. We have imprecise input data when the airgap becomes very small.

The computation overestimates the current at steady state, well after the time of the closing. This is explained by the fact that the resistance of the coil was kept constant during the modelling. In reality, the resistance of the coil at the end of the steady state was measured at 75 Ohm, a value 4% higher than the one before operation.

There is a good reproducibility of the measurements. The results of the 3D time transient modelling show a good agreement with measurements, especially for the closing time and the peak current during the closing process. This test case enables us to validate the new feature.

VI. CPU TIME AND MODELLING

The modelling of the actuator was performed on a PC with a clock speed of 800 MHz and enough RAM to avoid any need for disk access during the computation. We ran two types of computation, the commonly done 3D multi-static computation yielding independent static pictures of the device, to validate the force on the blade versus position and the 3D time transient computation with external circuit and mechanical connections.

The mesh applied for the device is a second order curvilinear mesh with 38,996 nodes. This mesh is obviously the initial mesh as the compressible part of the domain is re-meshed for each sample (time or position). But the total number of nodes does not change very much.

The multi-static computation was performed for 13 position samples and took approximately one hour of CPU. The time transient computation was performed for 83 time samples and took 10 hours. However, tt is important to note that if multi-static computations were done to obtain an equivalent circuit scheme of the device, a sampling of the current and of the position would be necessary, leading to probably more than 100 samples (10 current samples x 10 position samples). The time needed to perform this computation would exceed the time needed to perform the fully coupled computation.

Furthermore, all of the nonlinearities and motion effects are included in the fully coupled model.

VII. CONCLUSION

We have presented a new modelling scheme to increase the capabilities of FEM tools to handle motion in 3D problems. We can now model accurately both translating and pivoting motion, either with limited re-meshing or none at all. Any re-meshing is performed automatically during the solving. This new motion feature can be used to compute multi-static, constant speed or fully mechanically coupled problems. The methods and its implementations in a 3D tool have been validated on a test case in 2D and 3D, as well as on a real device. The computed values and the measurements show very good correlation.

These new features have been introduced into the 3D applications of FLUX, a commonly available CAD package.

VIII. REFERENCES

[1] C. Golovanov, J.-L. Coulomb, Y. Marechal, G. Meunier, “3D Mesh Connection Techniques Applied to Movement Simulation”, IEEE Trans. On Mag., Vol 34, N°3, 1998

[2] H. C. Lai, P. J. Leonard, D. Rodger, N. Allen, “3D Finite Element Dynamic Simulation of Elecftrical Machines Coupled to External Circuits”, IEEE Trans. On Mag., Vol 33, N°22, 1997

[3] K. Tani, T. Yamada, and Y. Kawase, “A new technique for 3D dynamic finite element analysis of electromagnetic problems with relative movement”, IEEE Trans. On Mag., vol 34, N° 5, pp. 3371-3374, 1998

[4] G. Meunier, S. Salon, J.L. Coulomb, and L. Krahenbuhl, “Hybrid finite element–boundary element solutions for 3D scalar potential problems”, IEEE Trans. On Mag., Vol 22, N°5, 1986

[5] K. Srairi, B. Benjima, M. Feliachi, and G. Develey, “Numerical and experimental studies of a linear electromagnetic actuator supplied by capacitor discharge voltages”, IEEE Trans. On Mag., vol 33, pp. 2061-2064, 1997

[6] K. Tani, T. Yamada, and Y. Kawase, “A new technique for 3D dynamic finite element analysis of electromagnetic problems with relative movement”, IEEE Trans. On Mag., vol 34, N° 5, pp. 3371-3374, 1998

[7] M. Jarnieux, P. Lombard, G. Reyne, G. Meunier, “Application of the Finite Element Method to the modelling of multi-sections Linear Induction Launchers”, in Proceedings of the 4th European Symposium on Electromagnetic Launch Technology, May 02-06 93, Celle-Germany

[8] V. Leconte, V. Mazauric, G. Meunier and Y. Maréchal, “Remeshing procedures compared to FEM-BEM coupling to simulate the transients of electromechanical devices”, in Proceedings of CEFC 2000, p 227

[9] V. Leconte, V. Mazauric, G. Meunier and Y. Maréchal, “Optimisation and sizing methodology for electromechanical actuators”, in Proceedings of ICEM 2000